INTERNATIONAL JOURNAL OF HYDROGEN ENERGY 39 (2014) 11547–11556

Available online at www.sciencedirect.com

ScienceDirect

journal homepage: www.elsevier.com/locate/he

Methanol and ethanol oxidation on carbon supported nanostructured Cu core Pt–Pd shell electrocatalysts synthesized via redox displacement

J.M. Sieben[*,1], *A.E. Alvarez, V. Comignani, M.M.E. Duarte* [2]

Instituto de Ingeniería Electroquímica y Corrosión, Universidad Nacional del Sur, B8000CPB Bahía Blanca, Argentina

ARTICLE INFO

Article history:
Received 19 March 2014
Received in revised form
11 May 2014
Accepted 19 May 2014
Available online 14 June 2014

Keywords:
Core–shell
Pt–Pd–Cu supported catalysts
Methanol
Ethanol and fuel cells

ABSTRACT

Six different carbon-supported Cu core Pt–Pd shell (Cu@Pt–Pd) catalysts have been successfully synthesized by the galvanic replacement of Cu atoms by Pt^{4+} and Pd^{2+} ions at room temperature and their electrocatalytic activity for methanol and ethanol oxidation have been evaluated in acid media. Cu@Pt–Pd core shell nanoparticles with a narrow size distribution and an average diameter in the range of 3.1–3.5 nm were generated onto the carbon support. The compositional and the structural analysis of the as-prepared materials pointed out that the nanoparticles are formed by a Cu rich core covered by a Pt–Pd rich shell due to the interdiffusion of the metals after the galvanic replacement reaction. The electrocatalytic properties of the Cu@Pt–Pd electrodes in the electro-oxidation of methanol and ethanol was found to be dependent on the electrochemical surface area, lattice strain of the surface, composition and thickness of the Pt–Pd shell surrounding the Cu core. The optimum catalyst composition to obtain the best performance for methanol and ethanol electro-oxidation was determined to be $Pt_{0.59}Pd_{0.324}Cu_{0.167}$/C (6.2 wt.% Pt, 2.2 wt.% Pd and 0.7 wt.% Cu). This catalyst has a greatly enhanced mass activity, lower onset potential and poisoning rate, and higher turnover number in the MOR and EOR reactions compared to a commercial $Pt_{0.51}Ru_{0.49}$/C (20 wt.% Pt and 10 wt.% Ru). Consequently, this simple preparation method is a viable approach to making a highly active catalyst with low platinum content for application in direct alcohol fuel cells (DAFCs).

Introduction

At present, the major bottlenecks for a widespread utilization of direct alcohol fuel cell (DAFC) technologies for stationary, portable and transportation applications are the high cost for market introduction, the reduced lifetime of the stacks and the low energy efficiency. A number of different strategies have been undertaken by the governments, technology providers and research institutions in order to reduce the cost of

* *Corresponding author*. Tel.: +54 291 4595100.
E-mail addresses: jmsieben@uns.edu.ar, jmsieben@yahoo.com.ar (J.M. Sieben).
[1] Member of CONICET, Argentina.
[2] Member of CIC, Argentina.

http://dx.doi.org/10.1016/j.ijhydene.2014.05.123

the most expensive parts of the stacks (*i.e.*, gas diffusion layer, membrane-electrode assembly and bipolar plates), to develop more stable membranes with reduced alcohol crossover and to increase the catalyst activity and platinum utilization.

In current electrodes of DAFCs more than half of the catalyst is inactive and the kinetic rate of the alcohol oxidation reaction is still rather slow [1,2]. The new strategies to prepare highly active and durable catalysts with low Pt loading (below 0.2 mg cm^{-2}) involves the production of multimetallic nanoparticles with a core–shell structure [3–10]. The core–shell architecture makes possible the design of catalysts with several unique properties just by choosing the metals that form the shell and core. These elements can be selected taking into account the segregation properties of the metals and their electronic and strain-inducing effects on the Pt surface atoms [11,12]. The most common and cost-effective method of fabricating core–shell nanoparticles is the galvanic displacement of a non noble metal (classically Cu) by platinum ions to leave Pt on the surface of the nanoparticles [9,13,14]. Sarkar et al. [13] and Zhu et al. [15] prepared a series of carbon-supported Pt–Cu nanoparticles catalysts with core–shell structure via chemical reduction method and subsequent galvanic replacement. The authors found an enhanced electrocatalytic activity for the oxygen reduction reaction on the core–shell electrodes compared to that found with commercial Pt catalysts. This observation was attributed to the electronic modification of the Pt shell by the inner Pt–Cu core. Recently, Chen et al. [6] reported that the activity of Ru core Pt shell nanoparticles in electro-oxidation of methanol is found to be dependent on the crystalline structure of the core and the lattice strain at the core–shell interface. Wan et al. [16] studied the electro-oxidation of methanol and the reduction of oxygen on Cu–Pd core Pt shell catalysts prepared by chemical reduction and galvanic displacement. The authors claimed that the enhanced activity of the core–shell electrodes with respect to Pt/C and PtRu/C is a result of improved Pt utilization. The electro-oxidation of ethanol in acid media on Cu@Pt carbon supported materials has been recently studied by Amman et al. [17]. The core–shell catalysts displayed a better activity with respect to Pt/C in terms of oxidation current and onset potential. They deduced that the Cu core and the presence of Cu atoms in the Pt lattice promote a different oxidation mechanism by preventing formation of adsorbed species originated from the decomposition of ethanol.

In a recent study, we have reported that several Cu@Pt–Ru core–shell supported catalysts synthesized by galvanic displacement exhibit enhanced catalytic activity and higher tolerance to poisoning towards methanol and ethanol electrooxidation compared to a commercial Pt–Ru/C material with higher Pt loading [9]. In the present work, the synthesis of a series of carbon supported Cu@Pt–Pd core–shell catalysts via galvanic displacement of Cu by Pt^{4+} and Pd^{2+} ions was carried out. The structural, morphological and electrochemical characteristics of the as-prepared core–shell nanoparticles were studied by TEM, EDX, ICP, XRD and cyclic voltammetry. In addition, their electrocatalytic activities towards methanol and ethanol oxidation in acid media were evaluated and compared with respect to a commercial Pt–Ru/C.

Experimental

Chemical reagents

Hexachloroplatinic(IV) acid hexahydrate ($H_2PtCl_6 \cdot 6H_2O$, 40% Pt) and palladium(II) chloride ($PdCl_2$, 99%) were purchased from Sigma–Aldrich, while copper(II) sulfate anhydrous ($CuSO_4$, p.a.) was obtained from Merck. Potassium hydroxide (KOH, ≥85%) and sodium borohydride ($NaBH_4$, >94%) were also supplied by Sigma–Aldrich. Citrate buffer solution (pH = 3.0–3.5) was prepared by mixing 17.5 ml of a 0.1 M $Na_3C_6H_5O_7$ (99.9% from Anedra) solution and 232.5 ml of a 0.1 M $C_6H_8O_7$ (99.9% from Anedra) solution with 247 ml of bidistilled water. Sulfuric acid (96%) was obtained from Carlo Erba, while CH_3OH (99.9%), CH_3CH_2OH (99.9%) and isopropyl alcohol (>99.5%) were provided by J.T. Baker®. In addition, Nafion® 117 solution (5 wt.% in a mixture of lower aliphatic alcohols and water) was supplied by Sigma–Aldrich. All solutions were prepared with bidistilled water.

Pretreated Vulcan XC-72 R carbon black ($S_{BET} = 241\ m^2\ g^{-1}$, and $d_p = 40$ nm, Cabot Corp.) was used as substrate. The carbon pretreatment was carried out in 3 M HNO_3 solution at 60 °C for 3 h. The slurry was then cooled and its pH value was adjusted to 7.0 with 1.0 M KOH solution. The pretreated carbon powder was then filtered, washed with bidistilled water and ethanol, and dried in an oven at 60 °C overnight.

Catalysts synthesis

A series of trimetallic Pt–Pd–Cu core–shell catalysts supported over the pretreated carbon powder were synthesized by a two-step route. First, copper nanoparticles supported on the pretreated carbon were synthesized by reduction of the metal precursor with $NaBH_4$ in the buffered aqueous solution at room temperature. Briefly, a given amount of $CuSO_4$ was dissolved into 100 ml of sodium citrate/citric acid buffer solution under vigorous stirring. Following, 100.0 mg of Vulcan XC-72 R was added into the solution, and then sonicated for 60 min. After that, the metal precursor was reduced to give 60 wt.% Cu in carbon by adding solid $NaBH_4$ to the slurry in a reductant to metal weight ratio of 4:1. The Cu/C material was collected via suction filtration, washed thoroughly with bidistilled water and ethanol and finally dried at 70 °C overnight.

The Cu@Pt–Pd core–shell particles were prepared by galvanic displacement reaction of Cu with Pt and Pd. 100.0 mg of the as-prepared carbon supported Cu material were suspended in 100 ml of the sodium citrate/citric acid buffer solution and sonicated for 30 min. Afterward, appropriate amounts of $H_2PtCl_6 \cdot 6H_2O$ and $PdCl_2$ acidic aqueous solutions were added and left to react for 2 h under magnetic stirring. The solid product that remained at the end of the reaction was collected via suction filtration, washed with bidistilled water and ethanol and dried in an oven overnight. In order to remove any unreacted copper nanoparticle as well as any oxide formed due to the handling of the samples, the as-prepared samples were digested for 2 h by using 9 M H_2SO_4 solution [13]. Finally, the powders were filtered, washed repeatedly with bidistilled water and ethanol and dried in an

Table 1 – Nominal atomic ratios used during the galvanic replacement reaction and catalyst composition determined by ICP-AES.

Catalyst	Pt	Pd	Pt	Ru	Pd	Cu	C
	At. ratios		wt.%				
PPC1	55	45	2.6	–	1.3	0.5	95.6
PPC2	65	35	6.2	–	2.2	0.7	90.9
PPC3	45	55	10.6	–	6.2	0.9	82.3
PPC4	35	65	13.0	–	11.4	1.3	74.3
PPC5	45	55	17.8		10.2	1.5	70.5
PPC6	55	45	23.5	–	12.2	2.0	62.3
Commercial	–	–	20.0	10.0	–	–	70.0

oven at 70 °C overnight. The composition of the as-prepared catalysts and the nominal atomic ratios of Pt and Pd used during the synthesis are presented in Table 1.

Electrochemical characterization

Conventional three-compartment glass cells were used to run the electrochemical experiments at room temperature with a PAR 273 potentiostat/galvanostat controlled by software ECHEM-M270. The counter electrode was a platinum wire separated from the working electrode compartment by a porous glass diaphragm. The reference electrode was a saturated calomel electrode (SCE, +0.241 V vs. RHE) located in a Luggin capillary. The potentials mentioned in this work are referred to this electrode. The working electrode was prepared by dispersing 20 μl of catalyst ink over the surface of a polished to mirror glassy carbon rod (3 mm diameter). After that, the electrodes were dried at 60 °C for 30 min to ensure the catalyst binding to the glassy carbon support. The catalyst ink (1 mg ml^{-1}) was prepared as follows: 5 mg of catalyst powder were dispersed in 3.98 ml of bidistilled water, 1 ml of isopropyl alcohol and 20 μl of Nafion solution by sonication for 30 min. All solutions were deaerated by bubbling N_2 for 30 min and then the inert atmosphere was maintained over the solution during the tests.

The characterization of the as-synthesized materials was carried out by cyclic voltammetry (CV) experiments in 0.5 M H_2SO_4 at a scan rate of 50 mV s^{-1}. The stable voltammograms were obtained after 40 cycles. Thereafter, the electrode activity for the alcohols electro-oxidation was evaluated in 1 M MeOH or 1 M EtOH +0.5 M H_2SO_4 solutions by applying a potential sweep at a scan rate of 50 mV s^{-1}. Stationary measurements (chronoamperometry) were performed applying pulses from an initial potential of 0 V for 15 min. Current densities for methanol and ethanol electro-oxidation were normalized per milligram of Pt. A commercial Pt–Ru/C electrocatalyst (20 wt.% Pt and 10 wt.% Ru loading, Sigma Aldrich) was used for comparison.

Furthermore, the electroactive surface area of the different electrodes was estimated by copper underpotential deposition method (Cu-UPD). Experimental details have been described in a previous paper [18].

Physicochemical characterization

The morphology of the catalyst surface and the particle size were analyzed using transmission electronic microscopy (TEM, JEOL, 100CX II) operated at 200 keV. Bulk composition analysis was performed by an energy dispersive X-ray spectroscopy probe attached to a scanning electron microscope (SEM, JEOL 100). X-ray diffraction (XRD) patterns of the Pt–Pd–Cu/C catalysts were recorded over the 2θ region of 30–80° using a Rigaku Dmax III C diffractometer with monochromated CuKα radiation source operated at 40 keV and 30 mA at a scan rate of 0.05° s^{-1}. The peak profiles in XRD patterns of the catalysts were fitted with the pseudo-Voigt function, using non-linear least-squares refinement procedures based on a finite difference Marquardt algorithm and the lattice parameters were estimated using Bragg's law.

The amount of Pt, Pd and Cu deposited on the carbon substrate was estimated using inductively coupled plasma optical emission spectrometry ICP-AES (Shimadzu 1000 model III). For this purpose, 10.0 mg of each sample were digested in aqua regia for at least 10 h and filtered off to separate the carbonaceous material from the solution containing the metal ions.

Results and discussion

Materials characterization

Table 1 presents the composition of the electrodes, as a weight percentage, with respect to the carbon support. The ternary

Table 2 – Characterization parameters of the as-prepared core–shell and commercial catalysts.

Catalyst	Pt	Ru	Pd	Cu	a_{fcc}	[b]d_c	[c]d_p	[d]ECSA
	[a]At.%				nm			$m^2\ g^{-1}_{Pt+Pd}$
PPC1	38.9	–	36.8	24.3	0.3911	3.1	3.22	67.9
PPC2	50.9	–	32.4	16.7	0.3891	2.9	3.10	135.8
PPC3	43.0	–	46.0	11.0	0.3886	3.6	3.45	73.0
PPC4	34.5	–	55.4	10.1	0.3892	4.0	3.55	54.8
PPC5	43.5	–	45.7	10.8	0.3913	3.5	3.55	47.8
PPC6	45.2	–	43.2	11.6	0.3892	3.4	3.20	40.0
Commercial	51.0	49.0	–	–	0.3918	3.0	2.90	60.3

[a] From EDX and ICP-AES analysis.
[b] From XRD (Debye–Scherrer equation).
[c] From TEM.
[d] From Cu-UPD and ICP-AES analysis.

metal composition was confirmed by EDX (Table 2), showing that the Pt and Pd contents are very close to the nominal values used in the galvanic displacement reaction.

The atomic ratios determined by EDX and ICP analysis, as well as the average diameter particle (d_p) are summarized in Table 2. The platinum and palladium contents in the as-prepared catalysts are between 32 and 55 at.%, while Cu content is in the range of 10–24 at.%. The electrochemical surface area per unit mass (ECSA) of the catalysts were calculated to be in the range of 40–136 $m^2\ g^{-1}$, while the ECSA of the commercial material was in the order of 60 $m^2\ g^{-1}$. As can be observed, the ECSA reaches the maximum value (136 $m^2\ g^{-1}$) when the noble metals content (Pt + Pd) in the catalyst is 8.4 wt.% (PPC2) but then decreased gradually down to 40 $m^2\ g^{-1}$ with increasing noble metal content (PPC6, 35.7 wt.% Pt + Pd).

Fig. 1 presents the stabilized cyclic voltammetry response of the as-prepared Pt–Pd–Cu/C catalysts in N_2 purged 0.5 M H_2SO_4 solution at a sweep rate of 50 mV s^{-1}. The voltammograms display a well defined region of hydrogen adsorption/desorption which suggests that the surface of the nanoparticles is mostly composed of Pt and Pd atoms. The anodic peak current indicative of the dissolution of Cu from the lattice upon cycling was absent for all electrodes. This performance confirms the core–shell structure of the nanoparticles having Cu atoms in the core and Pt or Pd atoms forming the shell, which in turn prevents the oxidation of Cu as Cu^{2+} during the potential cycling. This behavior is very similar to that recently reported by Amman an Easton for Pt–Cu/C core–shell catalysts [17]. Furthermore, most of the voltammograms developed a broad shoulder region, at approximately 0.35 V, associated with the presence of oxygen moieties on the surface of the carbonaceous substrate.

Fig. 2 presents representative TEM images of the as-synthesized catalysts and the commercial material. The average particle sizes of the as-synthesized materials are enlisted in Table 2. The micrographies reveal the presence of a large amount of almost rounded nanoparticles with sizes in the range of 2.9–3.6 nm, which appear regularly distributed over the carbon support material, whereas the nanoparticles showed in the TEM image of the commercial Pt–Ru/C catalyst have diameters between 2.9 and 3.1 nm. Nevertheless, some small agglomerates with characteristic lengths in the range of 8–12.0 nm are also observed in Fig. 2(f and g). The minor change in particle size with the increase of platinum and palladium contents suggest a redox deposition process in which only the outermost copper layers are replaced by Pt and Pd atoms. Furthermore, the dissolution of Cu and deposition of platinum and palladium on the remaining Cu nanoparticles prevents to a great extent the formation of new agglomerates.

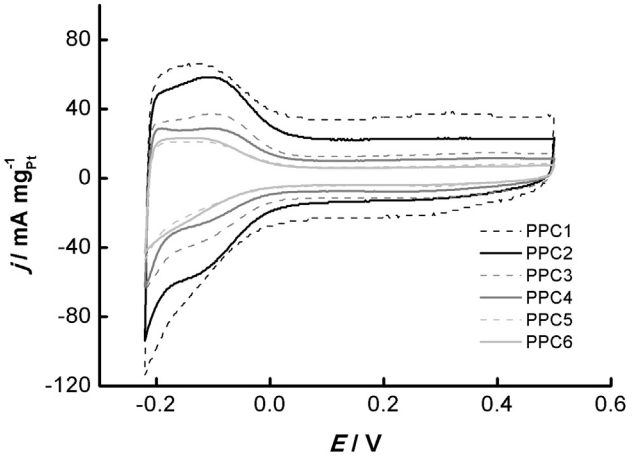

Fig. 1 – Stabilized cyclic voltammograms of the different Cu@Pt–Pd core–shell catalysts supported on Vulcan XC72R carbon black in 0.5 M H_2SO_4. $\upsilon = 50$ mV s^{-1}.

Therefore, the ECSA values reported in Table 2 could be interpreted in terms of the exposed percentage of Pt and Pd atoms available for the Cu-UPD reaction. In other words, the increase in Pt and Pd contents only results in thicker Pt–Pd layers on the core–shell nanoparticles. There exists however a discrepancy between the ECSA value of PCC1 and that expected for the noble metals content in this electrode. This disagreement could be due to a significant diminution of the available Pt and Pd sites at the nanoparticles surface because of the spontaneous interdiffusion process of the metals after the galvanic replacement reaction [19]; *i.e.* the migration of Pt and Pd atoms into the vacancies in the particle bulk and the migration of copper atoms from the core to the surface of the particles during this time, would result in less than an atomic layer of the noble metals at the nanoparticles surface.

The XRD diffraction patterns for the as-synthesized catalysts are shown in Fig. 3. The diffractograms of the as-prepared materials have three diffraction peaks centered at Bragg angles of about 40°, 47° and 69°, which can be assigned to the (111), (200) and (220) facets of the platinum and palladium face centered cubic (fcc) lattice structures. These three diffraction peaks appear slightly shifted toward higher 2θ values in the core–shell materials with respect to the corresponding peaks in pure Pt and Pd because of the difference in size between Pt, Pd and Cu. Furthermore, the XRD patterns do not show any peak corresponding to the fcc arrangement of Cu [20], which suggests the formation of a solid solution between Cu, Pt and Pd. Hence, it is assumed that the nanoparticles are composed of a Cu rich Pt–Pd–Cu core covered by a rich Pt–Pd shell [13]. This behavior has been also observed by several authors [19,21,22]. As was noted by Shibata et al. [19], for small nanoparticles (<5 nm) the metals are randomly distributed within the particle due to the interdiffusion across the core–shell interface, with the penetration of the surface atoms being dependent on both the core size and the total particle size.

Table 2 gives the lattice parameter values of all samples estimated by using Bragg's law. It can be noted that the as-prepared catalysts have smaller lattice constants compared to Pt (3.923 Å) and very close to that of Pd (3.8902 Å). Furthermore, the incorporation of Cu, which has a smaller atomic radius than Pt and Pd, induces the contraction of the Pt fcc network upon alloying, leading, therefore, to a decrease in the lattice parameter (or d-spacing).

Additionally Debye–Scherrer's equation [23] was used to estimate the average crystallite size of Pt–Pd–Cu/C and Pt–Ru/C catalysts from the (111) and (220) peaks centered at 2θ values of about 40° and 69°, respectively:

$$d_c = \frac{0.94\lambda_{K\alpha 1}}{B_{2\theta}\cos\theta_B} \quad (1)$$

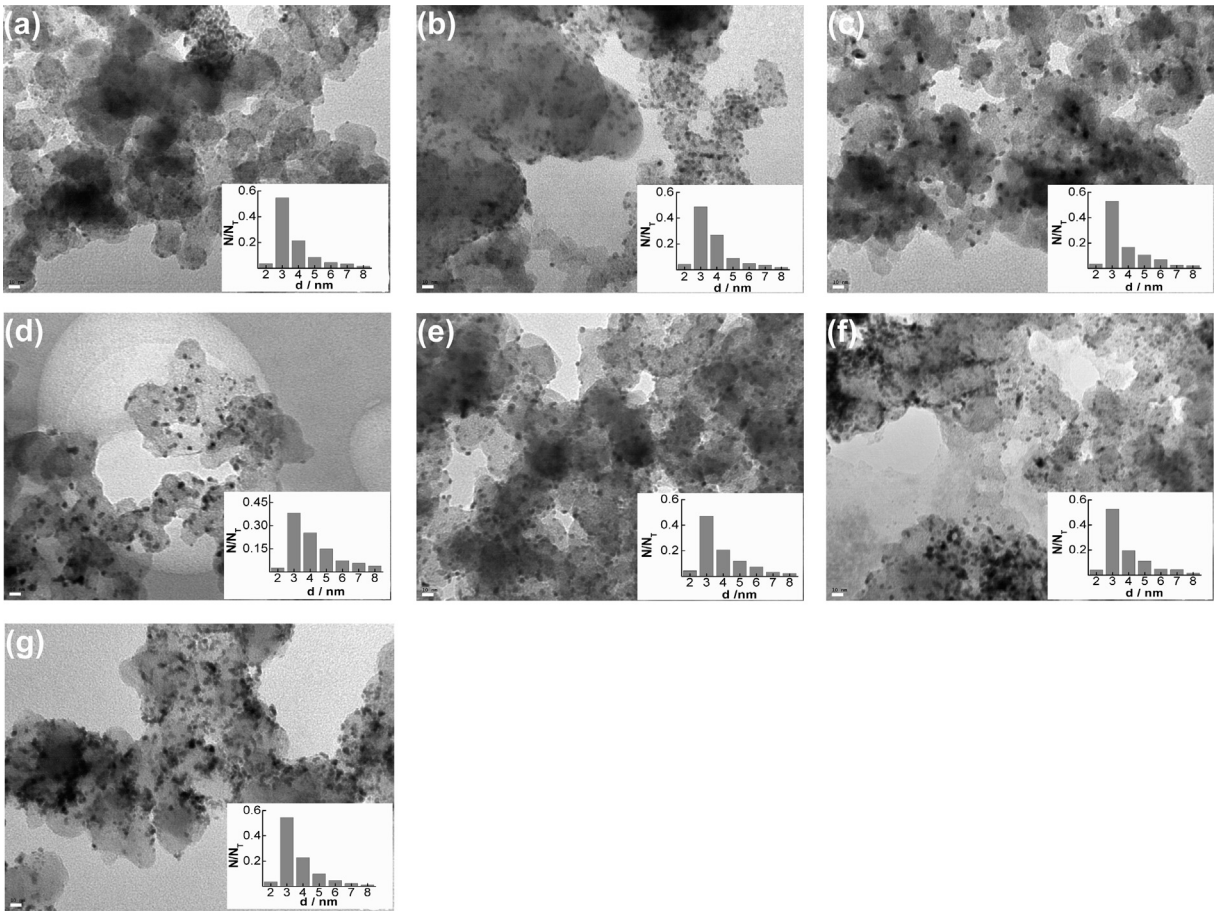

Fig. 2 – TEM images and histogram of particle size distribution of the as-synthesized Cu@Pt–Pt/C electrocatalysts used in this work: PPC1 (a), PPC2 (b), PPC3 (c), PPC4 (d), PPC5 (e) and PPC6 (f); and Pt–Ru/C catalyst (g).

where, $\lambda_{K\alpha 1}$ is the wavelength of X-ray, θ_B is the angle of the peak, and $B_{(2\theta)}$ is the full width at half-maximum (FWHM) of the peak broadening in radians and the value 0.94 comes from considering spherical crystallite geometry (or cubo-octahedral shape). The average crystallite size of the Pt–Pd–Cu/C catalysts falls in the range of 3.0–3.5 nm. Furthermore, the commercial Pt–Ru/C catalyst has a crystallite diameter of 3.0 nm. The crystallite sizes determined by Debye–Scherrer's equation are in good agreement with the previous TEM results.

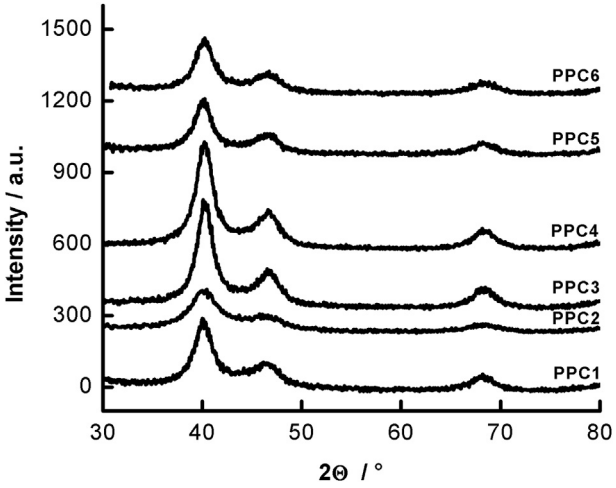

Fig. 3 – XRD diffractograms of the as-prepared catalysts and Pt–Ru/C by Sigma Aldrich.

Electrochemical performance of the as-prepared Pt–Pd–Cu catalysts

The steady cyclic voltammetry curves recorded for methanol and ethanol electro-oxidation in acid media at the as-synthesized trimetallic catalysts at room temperature are shown in Fig. 4(a and b), respectively. Insets of Fig. 4(a and b) shows the comparison between the mass activity of the most active as-prepared catalyst, PPC2, and the commercial Pt–Ru/C.

Interestingly, the onset potential of the as-synthesized catalysts for the methanol oxidation reaction (MOR) is slightly lower to that of the commercial Pt–Ru/C material. This means that the incorporation of Cu and Pd have a favorable activation effect in the electro-oxidation of the alcohol. The onset potential of methanol oxidation for PPC2 electrode is found to be 0.19 V, and it is shifted gradually to more positive potentials with the increase in platinum and palladium contents (up to 0.25 V for PPC6). However, the onset potential for PPC1 is very similar to that of PPC6 electrode. The

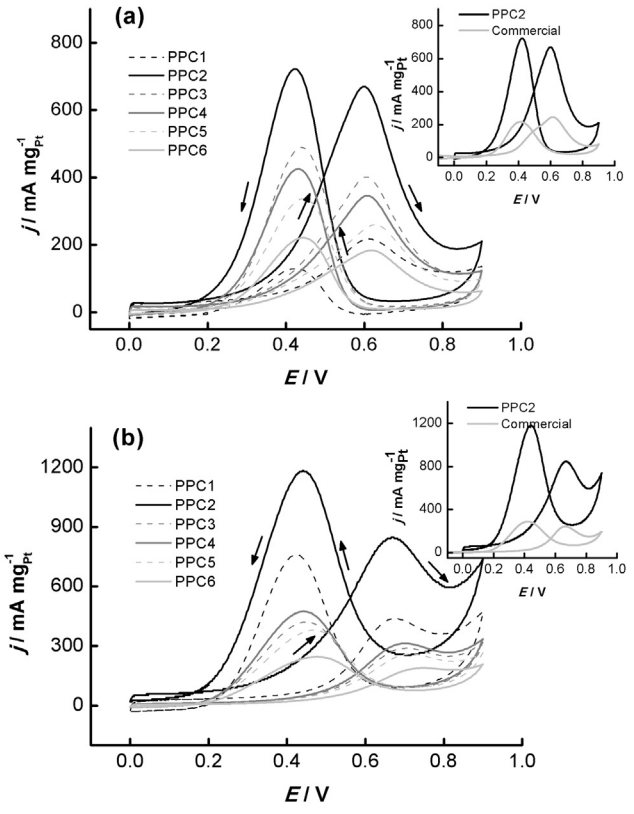

Fig. 4 – Stabilized cyclic voltammograms for the different electrode materials in 1 M CH_3OH/0.5 M H_2SO_4 (a), and 1 M CH_3CH_2OH/0.5 M H_2SO_4 (b) at room temperature. The sweep rate was 50 mV s^{-1} and the arrows indicate the scan direction. Insets: comparison between PPC2 and Pt–Ru/C.

voltammetric curves also indicated that PPC2 has the highest activity over the entire potential range, and the electrocatalytic activity for methanol oxidation decreases in the order PPC3 > PPC4 > PPC5 > PPC1 > PPC6. Moreover, the current density of PPC2 electrode is almost three times higher than that of Pt–Ru/C over the whole forward scan. The peak current density at PPC2 electrode is reached at 0.59 V, about 30 mV more negative than that at the commercial Pt–Ru/C catalyst, indicating that the alcohol oxidation is facilitated and needs less overpotential with this electrode. Further increase of Pt and Pd contents in the core–shell materials shifts the position of the anodic peak towards more positive potentials up to values very close to that at the commercial material (~0.62 V at PPC6).

On the other hand, the onset of the ethanol oxidation reaction (EOR) for PPC2 is shifted about 18 mV to a more positive potential value than that observed for MeOH oxidation, while the oxidation reaction starts at about 0.4 V for the commercial catalyst (Fig. 4(b)). As in the case of methanol electro-oxidation, a gradually shift of the onset potential in the direction of more positive values with the noble metal contents is noted down with the other as-synthesized electrodes. In the present case, the PPC2 electrode has the greatest activity for ethanol electro-oxidation and the intensity of the anodic current during the forward scan is found to follow the order of PPC1 > PPC4 ≥ PPC3 > PPC5 > PPC6. Furthermore, the electrocatalytic activity of PPC2 is as high as ten times that of Pt–Ru/C at the low potential region (0.3–0.4 V, a relevant region for fuel cells operation). However, this current density improvement is reduced by more than a half in the potential region close to the oxidation peak. This change may be explained by the difference in the nature of the synergistic effects of Ru, Pd and Cu atoms on the Pt-based catalysts. In the case of the commercial catalyst, the facilitation of ethanol oxidation reaction is produced via oxygen-containing species adsorbed on Ru atoms (bifunctional mechanism), whereas the presence of Pd and Cu atoms on the Pt-based core–shell material modifies the electronic structure of Pt atoms by a change in the electronic density of state at the Fermi level that weakens the adsorption of CO and other intermediates species, limiting catalysts poisoning [9,14,24]. It is also noted that the oxidation peak potential for both electrodes are very similar (~0.67 V). However, the peak potential of ethanol oxidation is observed at more positive potential values than those reported for the electro-oxidation of methanol (between 50 and 90 mV for Pt–Ru/C and PPC2, respectively). Also the progressive increment of Pt and Pd contents causes a shift of the peak potential to more positive compared with that on the Pt–Ru/C.

As can be seen from the above analysis, except for PPC1 electrode, the core–shell catalysts depict similar trends for the electro-oxidation of methanol and ethanol, *i.e.* the electrocatalytic activity of the as-synthesized electrodes decreased with an increase in the noble metals content due to the increase in Pt and Pd contents only results in thicker Pt–Pd layers on the core–shell nanoparticles and lower specific surface areas. These results are in good accordance with those reported in the literature [14]. On the other hand, PPC1 has one of the lowest catalytic activities for methanol oxidation, while it exhibits the second highest performance for ethanol oxidation. This anomalous behavior can be ascribed to a dissimilar tolerance to poisoning of this electrode for methanol and ethanol oxidation. This means that the Cu-rich core strongly promotes the oxidation of ethanol by favoring the splitting of the C–C bond or limiting substantially the accumulation of ethanolic residues as a result of electronic and strain effects. On the contrary, the inability of Pd and Cu atoms to supply OH_{ads} species at the low potential region, which inhibits the oxidation of methanol by the earlier poison of the available Pt sites or slows up the alcohol adsorption/dehydrogenation process [25].

Furthermore, the results point out that PPC1 and PPC2 catalysts are more active for electro-oxidation of ethanol than methanol. It is therefore interesting to note that, for PPC1 and PPC2, the presence of the Cu core has a higher impact in the EOR activity than in the MOR activity. This must indicate that the electronic and lattice strain effects of Cu core and Cu atoms in the Pt–Pd sublayers have a more pronounced influence in the global oxidation mechanism of ethanol in acid media than in the MOR mechanism. As we have previously indicated, the lattice mismatch in the Pt rich shell and the modification of the surface electronic structure may catalyze the C–C bond cleavage and consequently increases the efficiency of ethanol conversion to CO_2. On the contrary, the catalysts with higher Pt and Pd contents have higher activity

for MOR than EOR, which means that the Cu core has a very low impact in the catalytic process probably due to the thicker Pt–Pd shell. This behavior is in good agreement with results reported in the literature [26–28]. For instance, Kadirgan et al. [26] and Ozturk et al. [27] observed that Pt–Pd/C catalysts exhibited higher electrochemical activity for oxidation of methanol than ethanol in acid media. Liu et al. [28] also reported that some Pt–Pd alloy foam electrodes were more active for oxidation of methanol than ethanol.

In addition, the electrocatalytic performance in quasi-stationary conditions and the poisoning resistance of the as-prepared Pt–Pd–Cu/C and the commercial PtRu/C electrocatalysts were evaluated by chronoamperometric experiments at different constant potentials. The current–time curves of all electrodes at 0.4 V are shown in Fig. 5, and the electrocatalytic activities at different constant potentials are summarized in Fig. 6. It is noted that the electrodes have the same behavior as in the previous CV experiments, but the current densities obtained in the *j*-*t* curves are lower than those obtained in the CV experiments due to the partial blocking of the active sites by the accumulation of poisoning species such as CO, CH_3COOH, CH_3CHO, etc. [29–31]. The area-specific activities of the electrodes towards methanol and ethanol oxidation at 0.4 V are gathered in Table 3. Overall, the PPC2 electrode exhibits the highest current densities in comparison with the other as-prepared catalysts. Furthermore, the PPC2 electrode depicts catalytic activities 25% higher than that of Pt–Ru/C (0.121 vs. 0.095 mA cm^{-2}_{Pt-Pd} for methanol oxidation and 0.146 vs. 0.116 mA cm^{-2}_{Pt-Pd} for ethanol oxidation). Moreover, the as-prepared catalysts with similar or smaller ECSA to the Pt–Ru/C catalyst also display enhanced area-activities than the commercial Pt–Ru/C electrode. This behavior can be associated with the electronic effects between Pt, Pd and Cu atoms and the high number of surface defects in the Pt–Pd shell.

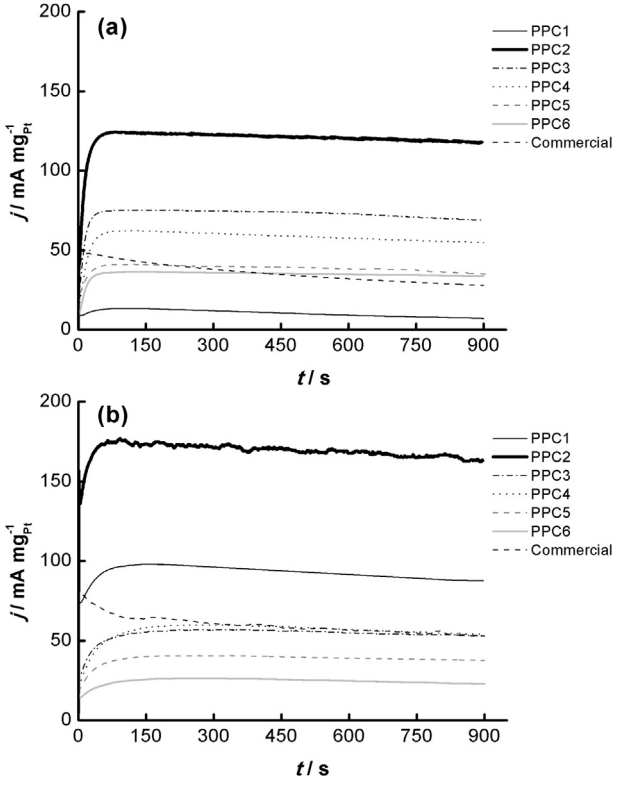

Fig. 5 – Chronoamperometry curves at 0.4 V vs. SCE for as-prepared electrodes and Pt–Ru/C in 1 M CH_3OH/0.5 M H_2SO_4 (a), and 1 M CH_3CH_2OH/0.5 M H_2SO_4 (b) at room temperature.

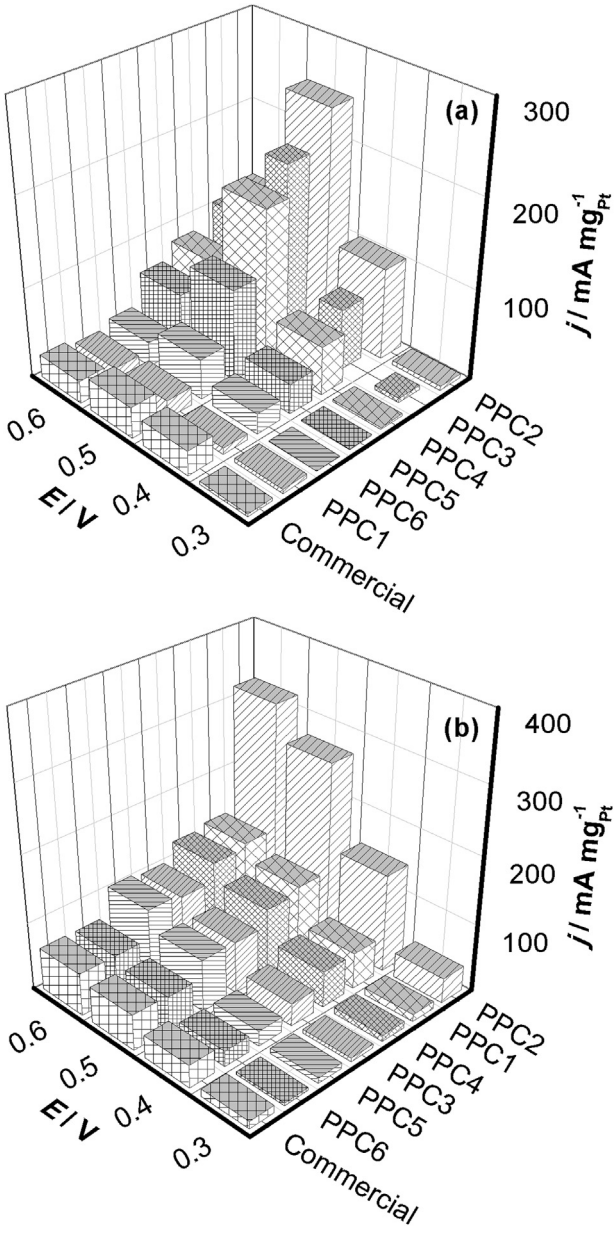

Fig. 6 – Electrocatalytic performance of the electrodes in M CH_3OH/0.5 M H_2SO_4 (a), and 1 M CH_3CH_2OH/0.5 M H_2SO_4 (b). Data taken from potentiostatic experiments at various potentials after 15 min.

In all chronoamperometric curves there is an initial current drop during the first 200 s followed by a relatively slower decay. Jiang and Kucernak [32] have indicated that the chemisorption of poisoning species originates the fast drop in the current density at short times, while the low current decay at longer times is ascribed to anion adsorption. These authors proposed to quantify the poisoning rate (δ) of the different

Table 3 – Poisoning rate and turnover number and area-specific activities of Pt–Pd–Cu/C and Pt–Ru/C electrodes for methanol and ethanol oxidation in 1 M MeOH or 1 M EtOH/0.5 M H_2SO_4 at different potentials.

Catalyst	CH_3OH						CH_3CH_2OH					
	0.4 V			0.5 V			0.4 V			0.5 V		
	δ $\%s^{-1}$	TON molec. $site^{-1}$ s^{-1}	j $\mu A\ cm^{-2}_{Pt+Pd}$	δ $\%\ s^{-1}$	TON molec. $site^{-1}$ s^{-1}	j $\mu A\ cm^{-2}_{Pt+Pd}$	δ $\%s^{-1}$	TON molec. $site^{-1}$ s^{-1}	j $\mu A\ cm^{-2}_{Pt+Pd}$	δ $\%s^{-1}$	TON molec. $site^{-1}$ s^{-1}	j $\mu A\ cm^{-2}_{Pt+Pd}$
PPC1	0.057	0.007	9.0	0.059	0.019		0.035	0.027	69.8	0.041	0.046	
PPC2	0.016	0.095	120.5	0.018	0.171		0.015	0.058	145.5	0.016	0.093	
PPC3	0.013	0.093	115.9	0.016	0.169		0.012	0.050	127.6	0.014	0.089	
PPC4	0.015	0.091	113.4	0.017	0.163		0.017	0.052	128.6	0.017	0.084	
PPC5	0.013	0.079	98.5	0.015	0.159		0.014	0.052	128.6	0.016	0.090	
PPC6	0.010	0.089	110.1	0.013	0.168		0.015	0.051	127.7	0.015	0.081	
Commercial	0.039	0.078	95.2	0.047	0.096		0.040	0.047	116.1	0.052	0.074	

electrodes in the electro-oxidation of methanol and ethanol by the following equation [32]:

$$\delta = \frac{100}{I_0}\left(\frac{dI}{dt}\right)_{t>500s} \quad (2)$$

where $(dI/dt)_{>500}$ is the slope of the linear portion of the current decay (A s^{-1}), and I_0 is the current at the start of polarization back extrapolated from the linear current decay (A). This parameter is tabulated in Table 3. The poisoning rate of all electrodes for methanol and ethanol electro-oxidation does not change significantly between 0.4 V and 0.5 V [33]. As it can be noted, the long-term poisoning rate of the as-synthesized catalysts (expect PPC1) is lower than that of Pt–Ru/C for both methanol and ethanol oxidation reaction. Furthermore, the poisoning rate parameter confirms the dissimilar tolerance to poisoning of PPC1 electrode for methanol and ethanol electro-oxidation.

The turnover frequency (TOF) or turnover number (TON) is an important figure of merit in heterogeneous catalysis because it permits the most accurate comparison of activity between catalysts with dissimilar compositions and structures [34]. This parameter can be defined as the rate of molecules converted per active surface site per second at a given potential and experimental condition [35]:

$$\mathrm{TON}\left(\frac{\text{molecules}}{\text{site s}}\right) = \frac{jN_A}{nF1.3\times10^{15}} \quad (3)$$

where, j is the steady-state current density (A cm^{-2}), n is the number of electrons produced by the oxidation of one alcohol molecule (6 and 12 e^- for methanol and ethanol conversion to CO_2, respectively), N_A is the Avogadro constant, F is the Faraday constant, and 1.30×10^{15} is the mean surface atomic density of the Pt-based catalysts (platinum sites per 1 cm^2 of the real surface area [35]). Table 3 also summarized the turnover numbers of the different catalyst materials at 0.4 V and 0.5 V. As can be noted the TON parameter increases as the applied potential increase because the electrodes becomes more active [32,36,37]. From Table 3, it can also be seen that the as-synthesized core–shell catalysts (except PPC1) have higher TON values than Pt–Ru/C for both alcohols, which means that these electrodes can oxidize more methanol or ethanol molecules during the same period of time using the same number of active sites than Pt–Ru/C. For instance, the number of methanol or ethanol reacting molecules on PPC2 increases between 20 and 45% with respect to Pt–Ru/C at an applied potential of 0.5 V. Sung et al. [36] reported TON values of 0.0827 and 0.059 molec. $site^{-1}$ s^{-1} for the electro-oxidation of 2 M MeOH/0.5 M H_2SO_4 on Pt–Ru–Ni (5:4:1) and Pt–Ru(1:1) unsupported catalysts at 0.65 V (NHE) and 25 °C. Recently, Ye et al. [38] reported a TON value of 0.89 molec. $site^{-1}$ s^{-1} for the oxidation of 1 M MeOH/0.5 M H_2SO_4 on Pt_4Au_1/ITO electrode at 0.75 V (SCE) and room temperature. However, in this study the measurements were performed at a polarization potential that is not relevant for fuel cells operation. Overall, the elevated TON values of the as-synthesized catalysts can be associated with the core–shell structure of the nanoparticles. The enhanced performance of core–shell electrocatalysts with respect to the conventional ones has been demonstrated by several authors [4,6,39].

When comparing the catalytic activity, poisoning rate and TON of the as-synthesized catalysts, it becomes evident that the increasing contents of platinum and palladium, *i.e.* the increasing thickness of the shell, limit the effects of the Cu core. This can be understood in terms of the electronic and lattice strain effects and the fraction of the surface Pt atoms exposed to the reaction. As a result, the optimum catalyst composition for methanol and ethanol electro-oxidation was determined to be $Pt_{0.59}Pd_{0.324}Cu_{0.167}$/C (6.2 wt.% Pt, 2.2 wt.% Pd and 0.7 wt.% Cu). Notably, this catalyst has greatly enhanced catalytic activity for the MOR and EOR reactions compared to commercial $Pt_{0.51}Ru_{0.49}$/C (20 wt.% Pt and 10 wt.% Ru). Note that the bifunctional effect is less important for this system because Pd and Cu have a more limited ability than Ru for breaking the water molecule to form OH_{ad} so the increase in activity and the turnover number TON, and the decrease in the poisoning rate are attributed to the higher electroactive surface area of the core–shell material and to ligand (*i.e.*, electronic effects due to the shift of Pt d-band position) and lattice strain effects [4,40,41].

The finding of this study suggests that the two-step process is a viable approach to making a highly active catalyst with good stability and low platinum content for application in direct alcohol fuel cells (DAFCs). However, further work should be done in order to understand how the MOR or the EOR mechanisms are influenced by the structure and composition of the Cu core/Pt–Pd shell supported catalysts.

Conclusions

The electrocatalytic activity for the methanol and ethanol oxidation reactions on carbon supported Cu@Pt–Pd core–-shell catalysts synthesized by a two-step process that involves a galvanic displacement reaction was investigated in acid media and compared with a commercial Pt–Ru/C catalyst. The synthesis method allowed us to prepare catalysts of different compositions but with similar average particle size, narrow particle distribution and electrochemical surface areas in the range of 40–136 $m^2\ g^{-1}$. The structural analysis of the as-prepared materials pointed out that the nanoparticles are composed of a Cu rich core covered by a Pt–Pd rich shell.

Cyclic voltammetry and chronoamperometry experiments indicated that the mass electrocatalytic activity of the as-synthesized electrodes decreased with an increase in the noble metals content due to the reduction of the fraction of Pt atoms in the catalyst surface exposed to the reaction (*i.e.*, reduction of the ECSA). The Cu core has only a high impact on the electrochemical properties of the catalysts with low Pt and Pd contents. On the contrary, the Cu core has a very low impact in the electrochemical properties of the materials with high Pt and Pd contents due to the thickness of the Pt–Pd shell. Overall, the electroactive surface area, the lattice strain of the surface layer, the composition and the thickness of the Pt–Pd shell surrounding the Cu core are decisive to achieve a high activity, a facilitated oxidation process and a low poisoning rate in the electro-oxidation of the alcohols.

The electrochemical investigations also revealed that the PPC2 electrode (6.2 wt.% Pt, 2.2 wt.% Pd and 0.7 wt.% Cu) exhibits a better performance towards MOR and EOR reactions compared to a commercial Pt–Ru/C sample with higher Pt loading, in terms of mass activity, onset potential, poisoning rate and turnover number. The outstanding performance of PPC2 was attributed to the high electrochemical surface area of the metallic catalyst, the lattice strain in the Pt–Pd shell and changes induced in the electronic properties of the Pt rich surface layer.

Acknowledgments

This work was supported by ANPCYT grant PICT-438. The authors are grateful to Graciela Mas for her assistance in the XRD measurements. V. Comignani acknowledges financial support from CONICET through a Ph.D. fellowship.

REFERENCES

[1] Léger JM, Coutanceau C, Lamy C. Electrocatalysis for the direct alcohol fuel cell. In: Koper MTM, editor. Fuel cell catalysis: a surface science approach. New Yersey: John Wiley & Sons; 2009. pp. 343–74.
[2] Vielstich W, Lamm A, Gasteiger HA. Handbook of fuel cells: fundamentals, technology and applications, vol. 2. New York: John Wiley & Sons; 2003.
[3] Long NV, Yang Y, Thi CM, Minh NV, Cao Y, Nogami M. The development of mixture, alloy, and core-shell nanocatalysts with nanomaterial supports for energy conversion in low-temperature fuel cells. Nano Energy 2013;2:636–76.
[4] Wang JX, Inada H, Wu L, Zhu Y, Choi YM, et al. Oxygen reduction on well-defined core-shell Nanocatalysts: Particle size, facet, and Pt shell thickness effects. J Am Chem Soc 2010;132:17664–6.
[5] Strasser P, Koh S, Anniyev T, Greeley J, More K, Yu C, et al. Lattice-strain control of the activity in dealloyed core-shell fuel cell catalysts. Nat Chem 2010;2:454–60.
[6] Chen TY, Luo TJM, Yang YW, Wei YC, Wang KW, Lin TL, et al. Core dominated surface activity of core–shell nanocatalysts on methanol electrooxidation. J Phys Chem C 2012;116:16969–78.
[7] Yan S, Zhang S. Methanol electrooxidation on carbon supported Aucore–Ptshell nanoparticles synthesized by an epitaxial growth method. Int J Hydrogen Energy 2012;37:9636–44.
[8] Kaplan D, Burstein L, Rosenberg Y, Peled E. Comparison of methanol and ethylene glycol oxidation by alloy and core–shell platinum based catalysts. J Power Sources 2011;196:8286–92.
[9] Sieben JM, Comignani V, Alvarez AE, Duarte MME. Synthesis and characterization of Cu core Pt–Ru shell nanoparticles for the electro-oxidation of alcohols. Int J Hydrogen Energy 27 May 2014;39(16):8667–74. http://dx.doi.org/10.1016/j.ijhydene.2013.12.064.
[10] Jiang X, Gür TM, Prinz FB, Bent SF. Atomic layer deposition (ALD) co-deposited Pt–Ru binary and Pt skin catalysts for concentrated methanol oxidation. Chem Mater 2010;22:3024–32.
[11] Zhang J, Lima FHB, Shao MH, Sasaki K, Wang JX, Hanson J, et al. Platinum monolayer on nonnoble metal-noble metal core-shell nanoparticle electrocatalysts for O_2 reduction. J Phys Chem B 2005;109:22701–4.
[12] Karan HI, Sasaki K, Kuttiyiel K, Farberow CA, Mavrikakis M, Adzic RR. Catalytic activity of platinum monolayer on

iridium and rhenium alloy nanoparticles for the oxygen reduction reaction. ACS Catal 2012;2:817–24.
[13] Sarkar A, Manthiram A. Synthesis of Pt@Cu core-shell nanoparticles by galvanic displacement of Cu by Pt^{4+} ions and their application as electrocatalysts for oxygen reduction reaction in fuel cells. J Phys Chem C 2010;114:4725–32.
[14] Xu C, Liu Y, Wang J, Geng H, Qiu H. Fabrication of nanoporous Cu-Pt(Pd) core/shell structure by galvanic replacement and its application in electrocatalysis. Appl Mater Interfaces 2011;3:4626–32.
[15] Zhu H, Li X, Wang F. Synthesis and characterization of Cu@Pt/C core–shell structured catalysts for proton exchange membrane fuel cell. Int J Hydrogen Energy 2011;36:9151–4.
[16] Wang H, Wang R, Li H, Wang Q, Kang J, Lei Z. Facile synthesis of carbon-supported pseudo-core@shell PdCu@Pt nanoparticles for direct methanol fuel cells. Int J Hydrogen Energy 2011;36:839–48.
[17] Ammam A, Easton EB. PtCu/C and Pt(Cu)/C catalysts: synthesis, characterization and catalytic activity towards ethanol electrooxidation. J Power Sources 2013;222:79–87.
[18] Sieben JM, Duarte MME, Mayer CE. Supported Pt and Pt–Ru catalysts prepared by potentiostatic electrodeposition for methanol electrooxidation. J Appl Electrochem 2008;38:483–90.
[19] Shibata T, Bunker BA, Zhang Z, Meisel D, Vardeman CF, Gezelter JD. Size-dependent spontaneous alloying of Au–Ag nanoparticles. J Am Chem Soc 2002;124:11989–96.
[20] Cheng WH. Reaction and XRD studies on Cu based methanol decomposition catalysts: role of constituents and development of high activity multicomponent catalysts. Appl Catal A 1995;130:13–30.
[21] Cochell T, Manthiram A. $Pt@Pd_xCu_y/C$ core–shell electrocatalysts for oxygen reduction reaction in fuel cells. Langmuir 2012;28:1579–87.
[22] Evteev AV, Levchenko EV, Belova IV, Murch GE. Interdiffusion and surface-sandwich ordering in initial Ni-core–Pd-shell nanoparticle. Phys Chem Chem Phys 2009;11:3233–40.
[23] Warren BE. X-ray diffraction. Massachusetts: Addison-Wesley, Reading; 1969.
[24] Bergamaski K, Gonzalez ER, Nart FC. Ethanol oxidation on carbon supported platinumerhodium bimetallic catalysts. Electrochim Acta 2008;53:4396–406.
[25] Antolini E, Gonzalez ER. Effect of synthesis method and structural characteristics of Pt–Sn fuel cell catalysts on the electro-oxidation of CH_3OH and CH_3CH_2OH in acid medium. Catal Today 2011;160:28–38.
[26] Kadirgan F, Beyhan S, Atilan T. Preparation and characterization of nano-sized Pt–Pd/C catalysts and comparison of their electro-activity toward methanol and ethanol oxidation] evaluated the electroactivity of Pt–Pd/C. Int J Hydrogen Energy 2009;34:4312–20.
[27] Ozturk Z, Sen F, Sen S, Gokagac G. The preparation and characterization of nano-sized Pt–Pd/C catalysts and comparison of their superior catalytic activities for methanol and ethanol oxidation. J Mater Sci 2012;47:8134–44.
[28] Liu J, Cao L, Huang W, Li Z. Direct electrodeposition of PtPd alloy foams comprised of nanodendrites with high electrocatalytic activity for the oxidation of methanol and ethanol. J Electroanal Chem 2012;686:38–45.
[29] Sieben JM, Duarte MME. Nanostructured Pt and Pt–Sn catalysts supported on oxidized carbon nanotubes for ethanol and ethylene glycol electrooxidation. Int J Hydrogen Energy 2011;36:3313–21.
[30] Sieben JM, Duarte MME. Methanol, ethanol and ethylene glycol electro-oxidation at Pt and Pt–Ru catalysts electrodeposited over oxidized carbon nanotubes. Int J Hydrogen Energy 2012;37:9941–7.
[31] Hamnett A. In: Wieckowski A, editor. Interfacial electrochemistry: theory, experiment, applications. New York: Marcel Dekker; 1999. p. 843.
[32] Jiang J, Kucernak A. Electrooxidation of small organic molecules on mesoporous precious metal catalysts II: CO and methanol on platinum/ruthenium alloy. J Electroanal Chem 2003;543:187–99.
[33] Jiang J, Kucernak A. Electrooxidation of small organic molecules on mesoporous precious metal catalysts I: CO and methanol on platinum. J Electroanal Chem 2003;543:153–65.
[34] Gasteiger HA, Kocha SS, Sompalli B, Wagner FT. Activity benchmarks and requirements for Pt, Pt-alloy, and non-Pt oxygen reduction catalysts for PEMFCs. Appl Catal 2005;56:9–35.
[35] Chrzanowaki W, Wieckowski A. In: Wieckowski A, editor. Interfacial electrochemistry: theory, experiment, applications. New York: Marcel Dekker; 1999. p. 950.
[36] Choi JH, Park KW, Kwon BK, Sung YE. Methanol oxidation on Pt/Ru, Pt/Ni, and Pt/Ru/Ni anode electrocatalysts at different temperatures for DMFCs. J Electrochem Soc 2003;150:A973–8.
[37] Jiang J, Kucernak A. Nanostructured platinum as an electrocatalyst for the electrooxidation of formic acid. J Electroanal Chem 2002;520:64–70.
[38] Ye W, Kou H, Liu Q, Yan J, Zhou F, Wang C. Electrochemical deposition of Au–Pt alloy particles with cauliflower-like microstructures for electrocatalytic methanol oxidation. Int J Hydrogen Energy 2012;37:4088–97.
[39] Zhou SH, Varughese B, Eichhorn B, Jackson G, Ilwrath KM. Pt–Cu core–shell and alloy nanoparticles for heterogeneous NO_x reduction: anomalous stability and reactivity of a core–shell nanostructure. Angew Chem Int Ed 2005;44:4539–43.
[40] Stamenkovic VR, Mun BS, Mayrhofer KJJ, Ross PN, Markovic NM. Effect of surface composition on electronic structure, stability, and electrocatalytic properties of Pt-transition metal alloys: Pt-skin versus Pt-skeleton surfaces. J Am Chem Soc 2006;128:8813–9.
[41] Koh S, Strasser P. Electrocatalysis on bimetallic surfaces: modifying catalytic reactivity for oxygen reduction by voltammetric surface dealloying. J Am Chem Soc 2007;129:12624–5;
Wang JX, Inada H, Wu L, Zhu Y, Choi YM, Liu P, et al. Oxygen reduction on well-defined core-shell nanocatalysts: particle size, facet, and Pt shell thickness effects. J Am Chem Soc 2009;131:17298–302.